



Excited-state quantum phase transitions and the entropy of the work distribution in the anharmonic Lipkin-Meshkov-Glick model

Haiting Zhang,¹ Yifan Qian,¹ Zhen-Xia Niu ^{1,*} and Qian Wang ^{1,2,†}

¹*Department of Physics, Zhejiang Normal University, Jinhua 321004, China*

²*CAMTP-Center for Applied Mathematics and Theoretical Physics, University of Maribor, Mladinska 3, SI-2000, Maribor, Slovenia*



(Received 31 October 2023; revised 10 March 2024; accepted 26 April 2024; published 4 June 2024)

Studying the implications and characterizations of the excited-state quantum phase transitions (ESQPTs) would enable us to understand various phenomena observed in quantum many-body systems. In this work, we delve into the affects and characterizations of the ESQPTs in the anharmonic Lipkin-Meshkov-Glick (LMG) model by means of the entropy of the quantum work distribution. The entropy of the work distribution measures the complexity of the work distribution and behaves as a valuable tool for analyzing nonequilibrium work statistics. We show that the entropy of the work distribution captures salient signatures of the underlying ESQPTs in the model. In particular, a detailed analysis of the scaling behavior of the entropy verifies that it not only acts as a witness of the ESQPTs but also reveals the difference between different types of ESQPTs. We further demonstrate that the work distribution entropy also behaves as a powerful tool for understanding the features and differences of ESQPTs in the energy space. Our results provide further evidence of the usefulness of the entropy of the work distribution for investigating various phase transitions in quantum many-body systems and open up a promising way for experimentally exploring the signatures of ESQPTs.

DOI: [10.1103/PhysRevE.109.064110](https://doi.org/10.1103/PhysRevE.109.064110)

I. INTRODUCTION

Excited-state quantum phase transitions (ESQPTs) [1–5] are a generalization of the ground-state quantum phase transitions (QPTs) [6,7] and have triggered numerous investigations in understanding their effects and signatures in a wide variety of quantum many-body systems, such as the Dicke model [8–12], the Rabi model [13,14], the periodically driving systems [15,16], the spinor Bose-Einstein condensates [17–19], the Lipkin-Meshkov-Glick (LMG) model [3,20–28], and the Kerr nonlinear oscillator [29,30], to name a few. In particular, ESQPTs have been experimentally observed in the superconducting microwave billiards [31] and the quantum gas [32]. ESQPTs are usually characterized by the singularities in the density of states [3–5] and play an important role in a diverse range of situations, including decoherence process [33,34], quantum quench dynamics [11,19,27–29,35–38], quantum chaos [10,39,40], quantum metrology [41], and dynamical tunnelling [42] as well as isomerization reactions [43]. Moreover, the efforts to identify the order parameters for ESQPTs [12,36] provide further understanding on their properties. Different aspects of ESQPTs have been reviewed in details in Ref. [5].

Recently, the anharmonicity-induced ESQPTs have attracted a lot of attention [43–47]. In contrast to the usual ESQPTs [3–5], which are associated with the ground-state QPTs, the anharmonicity triggering ESQPTs are independent of the ground-state QPTs and have different physical origin as

compared to the usual ones. It has been demonstrated that the onset of anharmonicity-induced ESQPTs is a consequence of the changes of the boundary in the finite-dimensional Hilbert space of the system [45,46]. It is worth mentioning that the finiteness of the Hilbert space of the system also results in another kind of ESQPTs, known as the static ESQPTs [9], which have no impacts on the system dynamics. The differences between the static and anharmonicity-induced ESQPTs have been pointed out in Ref. [46]. Both static and dynamical aspects of the anharmonicity-induced ESQPTs have been thoroughly investigated in several systems [45–47]. It was found that the anharmonicity-induced ESQPTs exhibit similar dynamical and static signatures as the usual ESQPTs. However, as two kinds of ESQPTs have different physical origins, it is natural to ask how to reveal their difference.

In the present work, we address this question by performing a detailed investigation on the scaling properties of the entropy of the quantum work distribution. As a measure of the complexity of the quantum work distribution, the work distribution entropy conveys a richness of information of the statistics of nonequilibrium quantum work, and particularly it can be used to diagnose the localization transition in Aubry-André-Harper model [48]. Moreover, due to the definition of the work distribution involves the spectrum of the system, one can expect that its entropy has ability to detect the presence of ESQPTs, as confirmed in Ref. [49]. Here, we further show that the entropy of the work distribution also enables us to distinguish different kinds of ESQPTs.

We carry out our study in the anharmonic LMG model [46,47], which is obtained by including an anharmonic term in the LMG model [46]. It was shown that in addition to the usual ESQPT observed in the LMG model, the

*niuzhx@zjnu.edu.cn

†qwang@zjnu.edu.cn

inclusion of the anharmonic term triggers a new ESQPT [46]. We demonstrate that both ESQPTs are characterized by the logarithmic divergence of the density of states at different critical energies. By analyzing the classical limit of the model, we perform a detailed analysis of the two ESQPTs and show how to understand them from the changes of the available phase space volume. To take the system out of the equilibrium state, we employ the sudden quench process. We show that the underlying ESQPTs leave a strong imprint in the nonequilibrium work statistics, resulting in a notable change in the behavior of the work distribution entropy. In particular, a detailed scaling analysis on the entropy demonstrates that two kinds of ESQPTs are manifested by different scaling exponents. Furthermore, for the sake of completeness, we discuss the energy dependence of the work distribution entropy and illustrate that it also behaves as a useful tool to detect the differences between ESQPTs in the energy space.

The remainder of the article is structured as follows. In Sec. II, we briefly review the definition and several features of the entropy of the work distribution. In Sec. III, we describe the anharmonic LMG model, discuss the signatures of ESQPTs in the model and study its classical counterpart. We analyze the physical origins of ESQPTs and obtain explicit expressions of their critical energies. In Sec. IV, we report our main results and show how the scaling behavior of the work distribution entropy distinguishes the different kinds of ESQPTs. We finally summarize our findings and discuss their potential extensions in Sec. V.

II. ENTROPY OF THE WORK DISTRIBUTION

Let us consider an isolated quantum system subjected to an external time-dependent driving of the control parameter in a time interval $[0, \tau]$. The system is initially prepared in a generic state ρ_i with initial Hamiltonian $H_i = \sum_n E_n^i |n_i\rangle\langle n_i|$. Here, $|n_i\rangle$ is the n th eigenstate of H_i and E_n^i is its corresponded eigenvalue. After the driving, the state of the system becomes $\rho_f = U \rho_i U^\dagger$, where U represents the unitary evolution. The driving process also changes system Hamiltonian from H_i to the final one $H_f = \sum_k E_k^f |k_f\rangle\langle k_f|$, where E_k^f is the eigenvalue of the k th eigenstate, $|k_f\rangle$, of H_f . The work done during this process is a random variable and is given by the energy difference between the final and initial Hamiltonians. Thus, to understand the nonequilibrium thermodynamics in the isolated quantum system, one needs to consider the work distribution rather than the work itself.

There are several different forms of the work distribution [50–56], depending on which scheme that is employed to evaluate the work during the process. Among them, we focus on the work distribution defined through the two-point measurement scheme [56–58], which is a most popular scheme for studying the work statistics in driven isolated systems [59–66]. The two-point measurement scheme consists of measuring the energy of the system at the beginning and at the end of the driving. Accordingly, the corresponding works, $W = E_k^f - E_n^i$, are distributed as

$$P(W) = \sum_{n,k} p_{k,n} \delta[W - (E_k^f - E_n^i)], \quad (1)$$

where $p_{k,n}$ denotes the joint probability of the two energy measurements and is given by

$$p_{k,n} = p_n^0 p_{k|n}^\tau, \quad (2)$$

with $p_n^0 = \langle n_i | \rho_i | n_i \rangle$ is the initial occupation probability and $p_{k|n}^\tau = |\langle k_f | U | n_i \rangle|^2$ are the transition probability between $|n_i\rangle$ and $|k_f\rangle$.

The work distribution for a quantum many-body system is complex. Hence, one usually studies the moments or cumulants of work, such as the mean and variance, in analyzing the work statistics of quantum systems [49,60–62,66–69]. Although the work moments or cumulants can capture several features of nonequilibrium thermodynamics in a variety of many-body systems, they cannot reveal the full information included in the work distribution. Very recently, a quantity that measures the complexity of $P(W)$ has been introduced, that is, the entropy of $P(W)$ [48]:

$$S_W = - \sum_W P(W) \ln[P(W)]. \quad (3)$$

It is easy to see that $S_W \in [0, \ln \mathcal{D}^2]$ with \mathcal{D} being the Hilbert space dimension of the quantum system. If the work is deterministic, then $S_W = 0$, while $S_W = \ln \mathcal{D}^2$ implies $P(W)$ is uniform.

It has been demonstrated that the entropy S_W unveils a richness information of the work distribution and provides a useful tool for understanding the nonequilibrium thermodynamics in quantum systems [48]. Moreover, the entropy also acts as a sensitive probe of the localization transition in the Aubry-André-Harper model. In this work, we use the entropy S_W to explore the implications of the ESQPT on the work distribution in the anharmonic LMG model. In particular, we explore how to distinguish different types of ESQPTs via the scaling properties of the work distribution entropy.

III. MODEL

As a generalization of the well-known LMG model [70–72], which describes N spin-1/2 mutual interacting particles in an external field and was widely studied in various areas [73–85], the anharmonic LMG model includes an anharmonic term and its Hamiltonian reads ($\hbar = 1$) [46,47]

$$H = \frac{2\gamma}{N} (J^2 - J_x^2) + (1 - \gamma) \left(J_z + \frac{N}{2} \right) - \frac{\alpha}{N} \left(J_z + \frac{N}{2} \right) \left(J_z + \frac{N}{2} + 1 \right), \quad (4)$$

where $J_{x,y,z} = \sum_{i=1}^N \sigma_i^{x,y,z}$ are the collective spin operators with $\sigma_i^{x,y,z}$ denote the i th spin Pauli matrices, $\gamma \in [0, 1]$ is the control parameter, and $\alpha > 0$ represents the strength of the anharmonic effect. The Hamiltonian (4) reduces to the original LMG model when $\alpha = 0$, while it includes the interactions between spins along z direction for $\alpha \neq 0$ cases.

One can easily show that the total spin $J^2 = J_x^2 + J_y^2 + J_z^2$ commutes with the Hamiltonian (4). Hence, we focus on the $j = N/2$ sector with the Hilbert space dimension $\mathcal{D}_{\mathcal{H}} = N + 1$. Moreover, the conservation of the parity $\Pi = e^{i\pi(J+J_z)}$ further allows us to split the Hilbert space into two subspaces, one has even parity with dimension $\mathcal{D}_{\mathcal{H}}^e = N/2 + 1$ and the

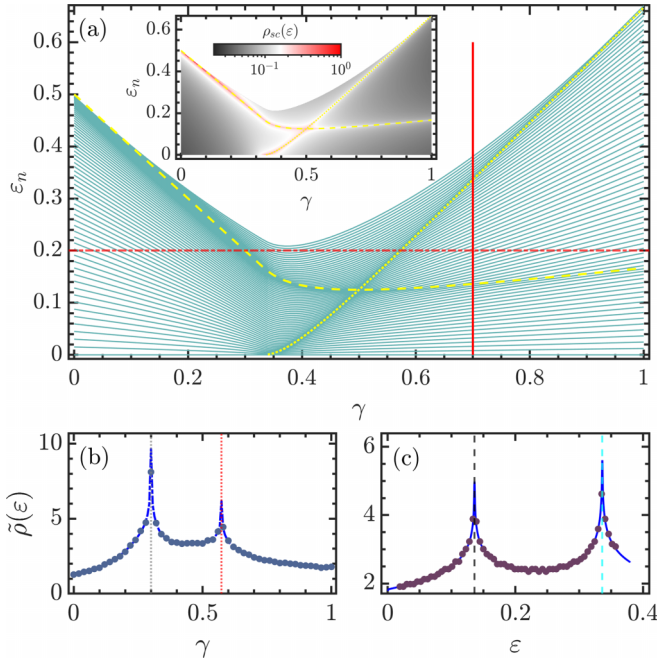


FIG. 1. (a) Rescaled even parity energy levels $\varepsilon_n = (E_n - E_0)/N$ of the anharmonic LMG model as a function of the control parameter γ for a system with $N = 2j = 130$. Inset: Semiclassical approximation of the density of states $\rho_{sc}(\varepsilon)$ [cf. Eq. (8)] as a function of ε_n and γ . Here, $\rho_{sc}(\varepsilon)$ has been normalized by its maximal value. The yellow dotted and dashed curves in main panel and inset indicate the ESQPTs critical energy $\varepsilon_{c,1}$ and $\varepsilon_{c,2}$, respectively. The horizontal red dot dashed line marks $\varepsilon = 0.2$, while the vertical red solid line indicates $\gamma = 0.7$. (b) Rescaled quantum density of states $\tilde{\rho}(\varepsilon) = \rho(E)/N$ as a function of γ along $\varepsilon = 0.2$ for the system size $N = 2j = 5000$. The blue dot dashed curve denotes $\rho_{sc}(\varepsilon)$, obtained from Eq. (8). The vertical red and gray dotted lines are the critical γ values of the ESQPTs provided by the equations $\varepsilon_{c,1} = \varepsilon_{c,2} = 0.2$. (c) Dependence of $\tilde{\rho}(\varepsilon)$ on ε along $\gamma = 0.7$ for the same system size as in panel (b). The blue solid curve represents $\rho_{sc}(\varepsilon)$ in Eq. (8), while the vertical cyan and black dashed lines are respective marks $\varepsilon_{c,1}$ and $\varepsilon_{c,2}$. In all panels, the anharmonicity parameter $\alpha = 0.5$. All quantities are unitless.

other is the odd parity subspace with dimension $\mathcal{D}_{\mathcal{H}}^o = N/2$. In this work, we restrict to the even parity subspace, which includes the ground state of the model.

It is known that the anharmonic LMG model undergoes a second-order ground-state QPT at $\gamma_c = 1/3$ and two ESQPTs, revealed by the clustering of the eigenlevels [46,47]. In Fig. 1(a), we plot how the rescaled excitation energies $\varepsilon_n = (E_n - E_0)/N$ vary as a function of the control parameter γ for a system with $N = 130$ and $\alpha = 0.5$. Here, E_n is the n th energy level with $n = 0$ being the ground state. Clearly, the energy spectrum of anharmonic LMG is more complex than the LMG model. One can see that the eigenlevels cluster along two different lines, which indicate the existence of two ESQPTs. The first ESQPT, marked by the yellow dotted line in Fig. 1(a), is the same as the one in the LMG model [23,27,35] and only appears for $\gamma > \gamma_c = 1/3$, while the second one, triggered by the anharmonic term, can exist in the entire range $\gamma \in [0, 1]$, as marked by the yellow dashed line

in Fig. 1(a). The clustering of the eigenlevels implies that both ESQPTs are characterized by a high density of states, $\rho(E) = \sum_n \delta(E - E_n)$. This is visible in Figs. 1(b) and 1(c), where we plot the rescaled density of states, $\tilde{\rho}(\varepsilon) = \rho(E)/N$, as a function of γ and ε , respectively, for a system size $N = 5000$ and $\alpha = 0.5$. It is easy to see that near the critical points of ESQPTs the density of states exhibits two remarkable peaks which will translate into the logarithmic divergences in the thermodynamic limit [27,46]. We would like to point out that the second ESQPT has strong impacts on system dynamics [47], in contrast to the static ESQPT introduced in Ref. [9].

The onset of ESQPT is closely connected to the changes of the available phase space in the underlying classical systems [3–5]. We therefore explore the classical limit of the anharmonic LMG model (4), to get a better understanding of the signatures of both ESQPTs.

A. Classical limit of the model

The classical counterpart of the Hamiltonian (4) is obtained from its expectation value with respect to the SU(2) spin coherent state [86–89] and normalized by the system size in the classical limit ($N \rightarrow \infty$). The final expression of the classical Hamiltonian is given by

$$\begin{aligned} \mathcal{H}_c(p, q) = & \frac{1 - \gamma}{4}(p^2 + q^2) - \frac{\gamma}{8}q^2(4 - p^2 - q^2) \\ & - \frac{\alpha}{16}(p^2 + q^2)^2 + \frac{\gamma}{2}, \end{aligned} \quad (5)$$

where $\{(p, q) | p^2 + q^2 \leq 4\}$ are the canonical variables.

The phase space structure of a classical model is determined by its fixed points [4,5], which are given by the solutions of equation $\nabla \mathcal{H}_c|_{(p_0, q_0)} = 0$. It is known that the classical system has a fixed point $(p_0, q_0) = (0, 0)$ with energy $\mathcal{E}_0 = \gamma/2$ for $\gamma < \gamma_c = 1/3$. However, as soon as $\gamma \geq 1/3$, the fixed points are given by $(p_1, q_1) = (0, \pm\sqrt{2(3\gamma - 1)/(2\gamma - \alpha)})$ with energy $\mathcal{E}_1 = \gamma/2 - (3\gamma - 1)^2/(8\gamma - 4\alpha)$. The energy difference $\mathcal{E}_1 - \mathcal{E}_0$ defines the ESQPT critical energy,

$$\varepsilon_{c,1} = \mathcal{E}_0 - \mathcal{E}_1 = \frac{(3\gamma - 1)^2}{4(2\gamma - \alpha)}, \quad \gamma \geq \gamma_c, \quad (6)$$

which is plotted as the yellow dotted line in Fig. 1(a).

Apart from above-mentioned fixed points, the anharmonicity gives rise to other fixed points $(p_2, q_2) = (\pm\sqrt{(2\gamma + 2 - 4\alpha)/\gamma}, \pm\sqrt{(4\alpha - 2 + 2\gamma)/\gamma})$ with energy $\mathcal{E}_2 = 1 - \gamma/2 - \alpha$ when $\gamma \geq |1 - 2\alpha|$. This indicates the occurrence of a new ESQPT with the critical energy,

$$\varepsilon_{c,2} = \begin{cases} \mathcal{E}_2 - \mathcal{E}_0 = 1 - \gamma - \alpha, & \gamma < \gamma_c, \\ \mathcal{E}_2 - \mathcal{E}_1 = \frac{(1 + \gamma - 2\alpha)^2}{4(2\gamma - \alpha)}, & \gamma \geq \gamma_c, \end{cases} \quad (7)$$

which is marked with the yellow dashed line in Fig. 1(a). As can be seen in Eq. (7), the critical energy $\varepsilon_{c,2}$ exists in the full range of γ value, unlike $\varepsilon_{c,1}$, which can only be found in the broken-symmetry phase $\gamma \in (\gamma_c, 1]$.

The presence of ESQPTs implies abrupt change in the behavior of the system available phase space volume. For the anharmonic LMG model, the available phase space volume is

given by [46]

$$\rho_{sc}(\varepsilon) = \frac{1}{4\pi} \int dpdq \delta[\varepsilon - \mathcal{H}_c(p, q)], \quad (8)$$

which can be considered as the semiclassical approximation of the quantum density of states [90]. In the inset of Fig. 1(a), we plot $\rho_{sc}(\varepsilon)$ as a function of γ and ε for $\alpha = 0.5$. One can clearly appreciate how the underlying ESQPTs leads to the singularities in the behavior of $\rho_{sc}(\varepsilon)$. The implications of ESQPTs are more visible in Figs. 1(b) and 1(c), where we show the variation of ρ_{sc} with γ and ε along the lines $\varepsilon = 0.2$ and $\gamma = 0.7$, respectively. We clearly see that $\rho_{sc}(\varepsilon)$ shows a sharp peak at the critical energies of ESQPTs. In fact, for the anharmonic LMG model with the classical counterpart has one degree of freedom, it was demonstrated that around the ESQPT critical energy $\rho_{sc}(\varepsilon)$ bears the logarithmic divergence, so that $\rho_{sc}(\varepsilon) \propto -\ln|\varepsilon - \varepsilon_c|$ [4,5]. Moreover, we also see an excellent agreement between the numerical results of $\tilde{\rho}(\varepsilon)$ and $\rho_{sc}(\varepsilon)$. This confirms that both ESQPTs are signified by the logarithmic divergences in the density of states as the system size goes to infinite.

In the following section, we investigate the impacts of these ESQPTs on the behavior of the entropy of the work distribution and discuss how to distinguish them via the scaling properties of the entropy.

IV. RESULTS

To analyze how two ESQPTs in the anharmonic LMG model affect the behavior of the entropy of the work distribution and to reveal their differences through the scaling properties of the entropy, we keep the value of α fixed and consider a sudden quench protocol. The initial state of the system is prepared in an eigenstate $|\psi_n^i\rangle$ of $H_i = H(\gamma_i)$ with energy E_n^i . At $t = 0$, a sudden quench takes place which changes γ from γ_i to $\gamma_f = \gamma_i + \delta\gamma$. The final Hamiltonian of the system is $H_f = H(\gamma_f) = \sum_k E_k^f |\psi_k^f\rangle\langle\psi_k^f|$, where $|\psi_k^f\rangle$ is the k th eigenstate of H_f with eigenvalue E_k^f . As $\rho_i = |\psi_n^i\rangle\langle\psi_n^i|$ is the n th eigenstate of H_i and the unitary operator $U = \mathbb{1}$ for the sudden quench process, the work distribution in Eq. (1) reduces to

$$P(W) = \sum_k p_{k,n} \delta[W - (E_k^f - E_n^i)], \quad (9)$$

where the joint probability in Eq. (2) simplifies to $p_{k,n} = |\langle\psi_k^f|\psi_n^i\rangle|^2$, namely, the transition probabilities between the initial and final states. Then, the entropy defined in Eq. (3) is given by

$$S_W = - \sum_W P(W) \ln[P(W)] = - \sum_k p_{k,n} \ln p_{k,n}. \quad (10)$$

Obviously, the entropy S_W now varies in the interval $S_W \in [0, \ln \mathcal{D}]$ with $S_W = 0$ corresponding to the deterministic work and $S_W = \ln \mathcal{D}$ implying $P(W)$ is uniform. Here, \mathcal{D} is the Hilbert space dimension of the system.

Since we aim to reveal the effects and differences of two ESQPTs, it is necessary to take the system passes through the critical energies of ESQPTs. This is achieved by tuning the quenching strength $\delta\gamma$, owing to the dependence of the energy in the post-quenched system on $\delta\gamma$ value. The critical

quenching is defined as the one that takes the post-quenched system to the ESQPT critical energy and denoted by $\delta\gamma_c$.

The critical quenching of an ESQPT can be obtained by using the mean field (semiclassical) approach. For the first ESQPT with the initial state is given by the ground state $|\psi_0^i\rangle$ of H_i , the critical quenching, $\delta\gamma_{c,1}$, can be written as

$$\delta\gamma_{c,1} = - \frac{(3\gamma_i - 1)(2\gamma_i - \alpha)}{2(3\gamma_i - 3\alpha + 1)}, \quad (11)$$

with $1/3 \leq \gamma_i \leq 1$. However, it was demonstrated that it is impossible to approach the second ESQPT when the system is initially in the ground state of H_i [47]. Alternatively, to reach the critical energy of the second ESQPT, the initial state should be set as the highest excited eigenstate, denoted by $|\psi_{n^*}^i\rangle$, of H_i [47]. Then, one can find that the critical quenching, $\delta\gamma_{c,2}$, of the second ESQPT is given by

$$\delta\gamma_{c,2} = \frac{4\alpha(1 - \gamma_i - \alpha) - (1 - \gamma_i)^2}{2(2\alpha + \gamma_i - 1)}, \quad (12)$$

where, again, $1/3 \leq \gamma_i \leq 1$. We emphasize that the conclusions in the present work are independent of the value of γ_i as long as $\gamma_i \in [1/3, 1]$.

In Fig. 2, we plot $P(W)$ for different rescaled quenching strengths, $\delta\gamma_a = \delta\gamma/\delta\gamma_{c,a}$ with $a = 1, 2$ for the first [Figs. 2(a)–2(c)] and second [Figs. 2(d)–2(f)] ESQPTs, with $\gamma_i = 0.7$, $\alpha = 0.5$, and $N = 2j = 800$. Overall, the behavior of $P(W)$ clearly unveils the two ESQPTs at $\delta\gamma_{c,1}$ and $\delta\gamma_{c,2}$. For both ESQPTs, when $\delta\gamma_a < 1$ the work distribution $P(W)$ has small support and shows significant population around the work value given by the energy difference between the ground states of H_f and H_i , as illustrated in Figs. 2(a) and 2(d). Conversely, as evidenced in Figs. 2(c) and 2(f), the support of $P(W)$ undergoes a remarkable increase for quenches that above the critical ones, i.e., $\delta\gamma_a > 1$. The particular dip observed in $P(W)$ for the critical quenches $\delta\gamma_a = 1$ [see Figs. 2(b) and 2(e)] not only marks the presence of ESQPTs, but also reflects the complexity of $P(W)$ at the ESQPTs critical points. However, we see that the work distribution is very regular when the quenching strength is far away from the critical value for both ESQPTs.

The above-observed features of $P(W)$ imply that the entropy of $P(W)$ should exhibit a drastic change as the system passes through the critical points of two ESQPTs. To see this, we plot S_W as a function of quenching strength and γ_i for two ESQPTs in Figs. 3(a) and 3(b). For both ESQPTs, one can clearly see that S_W exhibits quite different behaviors in different phases of an ESQPT. In particular, the entropy S_W is maximum around the critical point in both transitions. These properties of S_W are more visible in Figs. 3(c) and 3(d), where we show the dependence of S_W on the quenching strength with fixed γ_i for two ESQPTs.

The peak displayed in the behavior of S_W implies that it succinctly reveals the ESQPTs in the anharmonic LMG model and acts as a finite size precursor of an ESQPT. Hence, one can expect that in both transitions the location of the maximal entropy tends to the critical point and the entropy diverges in the thermodynamic limit $N \rightarrow \infty$. This is confirmed by Fig. 4, where we demonstrate how the position of the maximal S_W with respect to the critical value as well as the maximum value of S_W evolve with the system size N for different α and γ_i

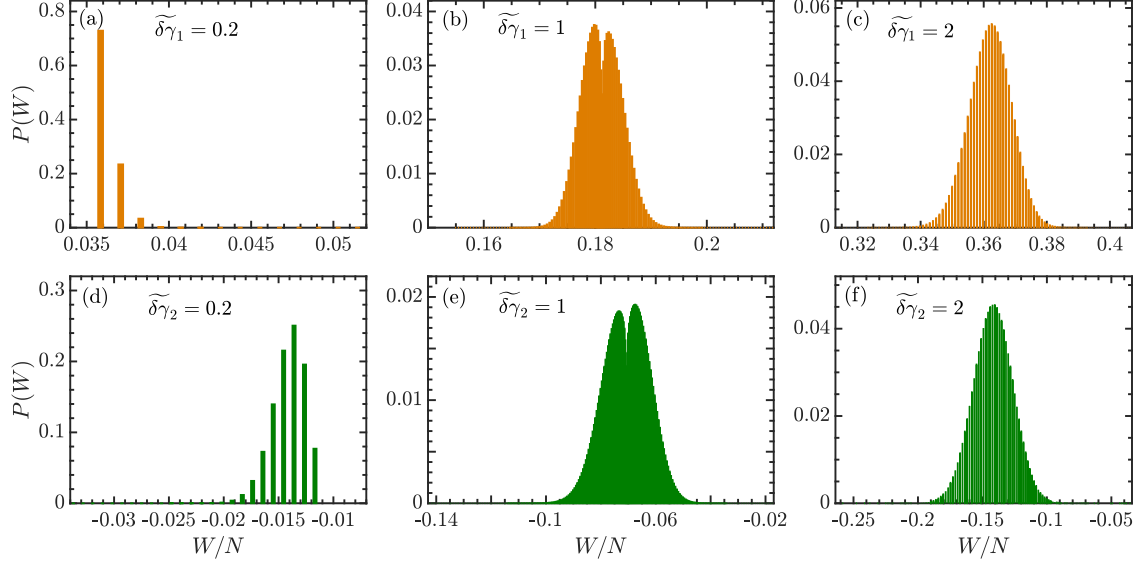


FIG. 2. Work distributions of the anharmonic LMG model (4). (a)–(c) $P(W)$ for the first ESQPT with different values of the rescaled quenching strength $\tilde{\delta\gamma}_1 = \delta\gamma/\delta\gamma_{c,1}$ and initial state is given by the ground state of H_i . Here, $\delta\gamma_{c,1}$ is obtained from Eq. (11). (d)–(f) $P(W)$ for the second ESQPT with several values of $\tilde{\delta\gamma}_2 = \delta\gamma/\delta\gamma_{c,2}$ and the initial state is the highest excited eigenstate of H_i . Here, $\delta\gamma_{c,1}$ is given by Eq. (12). In all panels, $\gamma_i = 0.7$, the anharmonicity parameter $\alpha = 0.5$, and the system size $N = 2j = 800$. All quantities are unitless.

cases in both transitions. Moreover, we find that the decrease of the distance between the location of the maximal S_W and the critical point with the increase of N follows power law

$$|1 - \tilde{\delta\gamma}_{a,m}| \propto N^{-\mu}, \quad (13)$$

where $a = 1, 2$ and $\tilde{\delta\gamma}_{a,m} = \delta\gamma_{a,m}/\delta\gamma_{c,a}$ with $\delta\gamma_{a,m}$ denoting the position of the maximal S_W for the first ($a = 1$) and/or

second ($a = 2$) ESQPT. Additionally, the fitting of the data shows that for both ESQPTs the divergence of the maximum value of S_W , denoted by $S_{W,m}$, is well captured by

$$S_{W,m} \propto \nu \ln N. \quad (14)$$

The values of the scaling exponents μ and ν for the two ESQPTs are shown in Table I. We see that for both transitions

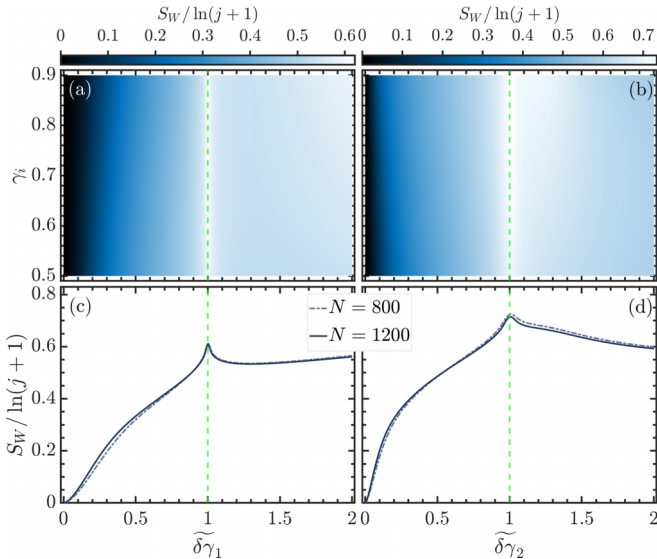


FIG. 3. (a), (b) Rescaled entropy of $P(W)$ as a function of $\tilde{\delta\gamma}_a = \delta\gamma/\delta\gamma_{c,a}$ ($a = 1, 2$) and γ_i for (a) the first ESQPT and (b) the second ESQPT with $N = 2j = 800$. Here, $\delta\gamma_{c,a}$ are obtained from Eqs. (11) and (12). (c), (d) Rescaled entropy of $P(W)$ as a function of $\tilde{\delta\gamma}_a$ for several system sizes, for (c) the first ESQPT and (d) the second ESQPT with $\gamma_i = 0.7$. The vertical green dashed line in each panel marks the critical quenching strengths $\delta\gamma_{c,a}$. In all panels, the anharmonicity parameter $\alpha = 0.5$. All quantities are unitless.

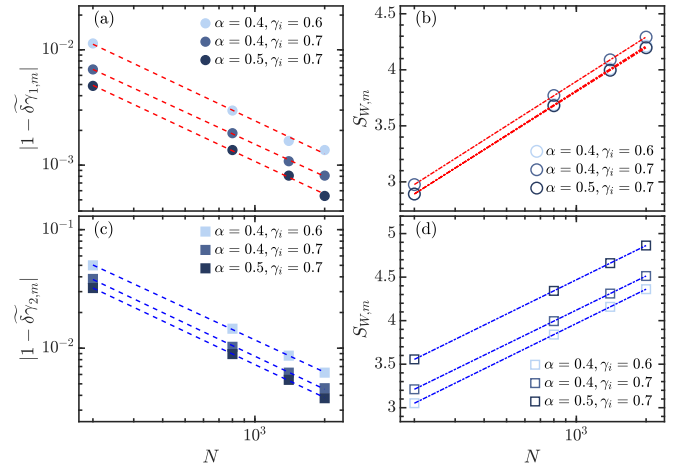


FIG. 4. (a) Distances of the rescaled quenching strength $\tilde{\delta\gamma}_{1,m}$ where the maximal S_W occurs to its critical value 1 versus system size N with several α and γ_i for the first ESQPT. (b) Maximum values of S_W , $S_{W,m}$, as a function of N for different values of α and γ_i of the first ESQPT. (c) Distances between $\tilde{\delta\gamma}_{2,m}$, where S_W reaches its maximal value, and 1 as a function of N for several α and γ_i of the second ESQPT. (d) Maximal values of S_W , $S_{W,m}$, versus N for different α and γ_i of the second ESQPT. The dashed lines in panels (a) and (c) correspond to the power-law scaling $N^{-\mu}$, while the dotted lines in panels (b) and (d) represent $\nu \ln N$. The explicit values of μ and ν are given in Table I. All quantities are unitless.

TABLE I. Scaling exponents μ and ν for the cases plotted in Fig. 4.

1st ESQPT			2nd ESQPT		
$\alpha = 0.4, \gamma_i = 0.6$	$\alpha = 0.4, \gamma_i = 0.7$	$\alpha = 0.5, \gamma_i = 0.7$	$\alpha = 0.4, \gamma_i = 0.6$	$\alpha = 0.4, \gamma_i = 0.7$	$\alpha = 0.5, \gamma_i = 0.7$
$\mu = 0.9496$	$\mu = 0.9280$	$\mu = 0.9432$	$\mu = 0.9043$	$\mu = 0.9262$	$\mu = 0.9251$
$\nu = 0.5732$	$\nu = 0.5719$	$\nu = 0.5670$	$\nu = 0.5688$	$\nu = 0.5651$	$\nu = 0.5679$

the exponent ν is almost independent of the values of α and γ_i and approximately given by $\nu \approx 0.57$, while the value of μ is different for two ESQPTs and varies with α and γ_i as well. This means that even though S_W exhibits a similar properties for both ESQPTs, its scaling behavior depends on the type of ESQPT. Hence, we can conclude that the scaling analysis of S_W would help us to distinguish different types of ESQPTs.

So far, we have focused on to investigate the impacts and differences of ESQPTs by means of the entropy of the quantum work distribution in the anharmonic LMG parameter space. However, the prominent signature of ESQPTs is the singularity in the density of states at the critical energy. Therefore, it is also necessary to explore whether the scaling of the work distribution entropy is also able to detect the differences between two ESQPTs in the energy space.

To this end, we still consider the sudden quench process. However, as we are currently interested in the energy dependence of the entropy of the work distribution, we fixed $\delta\gamma = 0.001$ and study the properties of the work distribution and its entropy for different eigenstates with fixed γ_i .

In Fig. 5, we report the work distribution of n th eigenstate, denoted by $P_n(W)$, for several excitation eigenlevels with $\gamma_i = 0.7$, $\alpha = 0.5$, and the system size $N = 2j = 800$, for the two

ESQPTs. Due to the very small value of $\delta\gamma$, the amount of work that is injected or extracted during the quench process is also very small. Nevertheless, for both transitions, obvious differences in the behavior of $P_n(W)$ between two phases of an ESQPT can be observed. At the critical energies of two ESQPTs, the highest density of states means that the critical eigenstates are very sensitive to the small perturbations. As a consequence, the work distribution $P_n(W)$ becomes more dense than the cases that far away from the critical energy, as seen in Figs. 5(b) and 5(e).

The behaviors of $P_n(W)$ demonstrated in Fig. 5 indicate that the entropy of $P_n(W)$, denoted by $S_W^{(n)}$, would be maximized at the ESQPT critical energy. We plot in Fig. 6(a) how the entropy $S_W^{(n)}$ evolves with γ_i and excitation energies ε_n . We note that the overall behavior of $S_W^{(n)}$ is very similar to $\rho_{sc}(\varepsilon)$, as seen by comparing Fig. 6(a) with Fig. 1(a). Importantly, one can clearly observe that the entropy $S_W^{(n)}$ has a peak along the critical energies of two ESQPTs. This is confirmed by the inset of Fig. 6(a), where we show how the positions of peaks in $S_W^{(n)}$ evolve as a function of ε_n and γ_i . An excellent agreement between the numerical and analytical results implies that $S_W^{(n)}$ behaves as a witness of two ESQPTs in the anharmonic LMG model. Further verifications of this statement are demonstrated in Figs. 6(b) and 6(c), where we illustrate the dependence of $S_W^{(n)}$ on γ_i with fixed ε_n and on

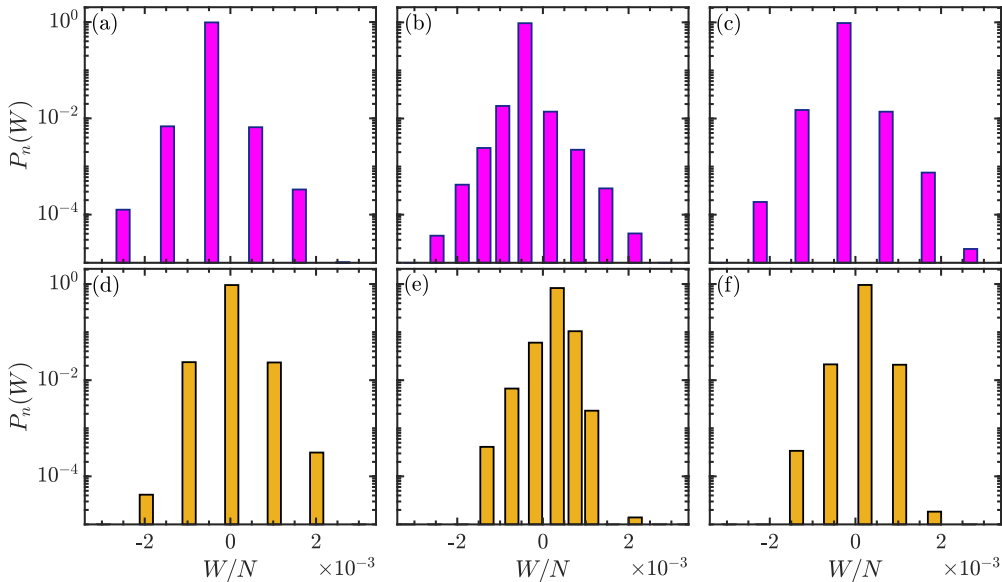


FIG. 5. Work distribution $P_n(W)$ of the n th eigenstate $|\psi_n\rangle$ for (a) $n = 79$, $\varepsilon_n \approx 0.094$, (b) $n = 129$, $\varepsilon_n \approx \varepsilon_{c,2} = 0.1361$, (c) $n = 179$, $\varepsilon_n \approx 0.179$, (d) $n = 279$, $\varepsilon_n \approx 0.2818$, (e) $n = 344$, $\varepsilon_n \approx \varepsilon_{c,1} = 0.3361$, and (f) $n = 371$, $\varepsilon_n \approx 0.3544$. Here, $\varepsilon_n = (E_n - E_0)/N$ with E_0 is the ground-state energy, $\varepsilon_{c,1}$ and $\varepsilon_{c,2}$ are, respectively, given by Eqs. (6) and (7). Other parameters: $\gamma_i = 0.7$, $\alpha = 0.5$, and $N = 2j = 800$. All quantities are unitless.

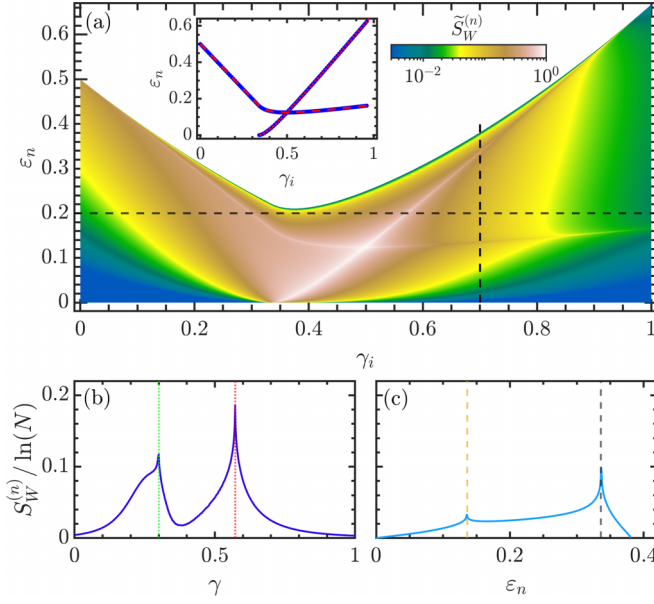


FIG. 6. (a) Normalized work distribution entropy, $\tilde{S}_W^{(n)} = S_W^{(n)}/S_{\max}^{(n)}$, as a function of γ_i and $\varepsilon_n = (E_n - E_0)/N$. Here, $S_{\max}^{(n)}$ denotes the maximal values of $S_W^{(n)}$ and E_0 is the ground-state energy. The horizontal and vertical dashed lines denote $\varepsilon_n = 0.2$ and $\gamma_i = 0.7$. Inset: Positions of the peaks in $S_W^{(n)}$ as a function of ε_n and γ_i . The red dotted and dashed curves in the inset mark the critical energies $\varepsilon_{c,1}$ and $\varepsilon_{c,2}$, given by Eqs. (6) and (7), respectively. (b) $S_W^{(n)}/\ln N$ as a function of γ_i along $\varepsilon_n = 0.2$. The vertical red and green dotted lines mark the critical values of γ_i obtained from $\varepsilon_{c,1} = \varepsilon_{c,2} = 0.2$. (c) $S_W^{(n)}/\ln N$ versus ε_n with $\gamma_i = 0.7$. The vertical gray and orange dashed lines correspond to $\varepsilon_{c,1}$ and $\varepsilon_{c,2}$. Other parameters: $\alpha = 0.5$, $\delta\gamma = 0.001$, and $N = 2j = 800$. All quantities are unitless.

ε_n with fixed γ_i , respectively. The above-observed features of $S_W^{(n)}$ lead us to believe that the presence of ESQPTs in the anharmonic LMG model can be reliably probed by the entropy of the quantum work distribution. However, both ESQPTs are signified by similar features of $S_W^{(n)}$, indicating that further scaling analysis of $S_W^{(n)}$ is required to distinguish two ESQPTs.

By taking the position of the peak in $S_W^{(n)}$, denoted by $\varepsilon_c(N)$, as an estimation of the critical energy of an ESQPT, we examine how it approaches the exact critical energy as the system size N is increased. In Figs. 7(a) and 7(b), we plot how the distance between $\varepsilon_c(N)$ and $\varepsilon_{c,a}$ varies as a function of N along with the numerical fitting of data for two ESQPTs. For both ESQPTs, we see that the convergence of $\varepsilon_c(N)$ to $\varepsilon_{c,a}$ with increasing N is well captured by the power law

$$|\varepsilon_c(N) - \varepsilon_{c,a}| \sim N^{-\mu_E(\gamma_i)}. \quad (15)$$

Here, the scaling exponent $\mu_E(\gamma_i)$ depends on the type of ESQPT and the value of γ_i . In addition, we also show the finite-size scaling analysis of the peak value of the entropy, denoted by $S_{W,m}^{(n)}$, for both ESQPTs in Figs. 7(c) and 7(d). One can see that $S_{W,m}^{(n)}$ is diverged as $N \rightarrow \infty$. Moreover, the fitting of the data demonstrates that the scaling behavior of $S_{W,m}^{(n)}$ with N is give by

$$S_{W,m}^{(n)} \sim N^{\nu_E(\gamma_i)}. \quad (16)$$

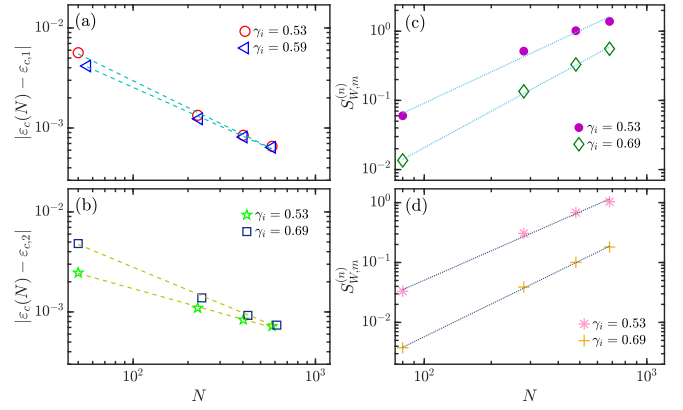


FIG. 7. (a), (b) Distances between the estimated critical energies $\varepsilon_c(N)$ and $\varepsilon_{c,a}$ as a function of the system size N for (a) the first ESQPT ($a = 1$) and (b) the second ESQPT ($a = 2$) with several γ_i . (c), (d) Maximal entropy, $S_{W,m}^{(n)}$, versus N for (c) the first ESQPT and (d) the second ESQPT with different γ_i . The dashed lines in panels (a) and (b) denote the power-law decay $|\varepsilon_c(N) - \varepsilon_{c,a}| \propto N^{-\mu_E(\gamma_i)}$, while the dotted lines in panels (c) and (d) represent $S_{W,m}^{(n)} \propto N^{\nu_E(\gamma_i)}$. Explicit dependence of $\mu_E(\gamma_i)$ and $\nu_E(\gamma_i)$ on γ_i are plotted in Fig. 8. Here, $\varepsilon_{c,1}$ and $\varepsilon_{c,2}$ are, respectively, given by Eqs. (6) and (7) with $\alpha = 0.5$. All quantities are unitless.

The scaling exponent $\nu_E(\gamma_i)$ is determined by the value of γ_i and the type of ESQPT. It is worth pointing out that the scaling behavior of $S_{W,m}$ in Eq. (14) is quite distinct from the one in Eq. (16).

Above results imply that the difference between the usual and anharmonic-induced ESQPTs are manifested in the different scaling exponents. The explicit dependence of $\mu_E(\gamma_i)$ and $\nu_E(\gamma_i)$ on the control parameter γ_i for two ESQPTs are displayed in Figs. 8(a) and 8(b), respectively. It is obvious that two ESQPTs can be clearly distinguished by the values

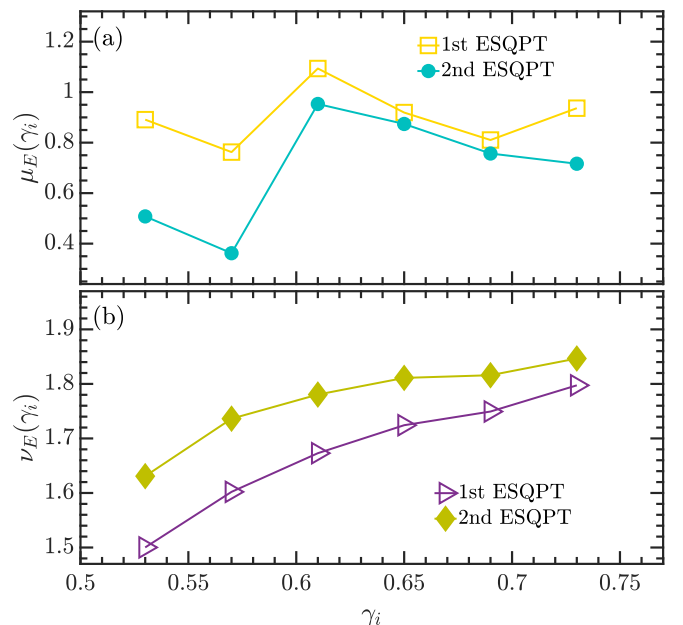


FIG. 8. (a) $\mu_E(\gamma_i)$ and (b) $\nu_E(\gamma_i)$ as a function of γ_i for the two ESQPTs. Other parameter: $\alpha = 0.5$. All quantities are unitless.

of the scaling exponents. Hence, the usefulness of the entropy of the quantum work distribution is twofold. On the one hand, it acts as a diagnostic tool to detect the presence of ESQPTs in various quantum systems. On the other hand, and importantly, its scaling analysis can help us to identify differences between different types of ESQPTs.

V. CONCLUSION

In conclusion, using the entropy of the quantum work distribution, we have discussed how to distinguish the usual and anharmonic-induced ESQPTs in the anharmonic LMG model. As a generalization of the well-known LMG model, the anharmonic LMG model includes an anharmonic term in the LMG Hamiltonian. As a consequence, in addition to the usual ESQPT, which is associated with the ground-state QPT and has been observed in the LMG model, a new ESQPT induced by the anharmonic term is present in the anharmonic LMG model.

To understand the new ESQPT, we have studied the classical limit of the model. We have shown that although the physical origins of two ESQPTs are different, both of them are signified by the logarithmic divergence of the density of states at their critical energies. We have performed the stability analysis of the classical Hamiltonian and derived the explicit form of the critical energies of two ESQPTs.

The entropy of the quantum work distribution measures the complexity of the work distribution. By focusing on the sudden quench process, we have demonstrated that the entropy is acutely sensitive to two ESQPTs, resulting in the presence of sharp peaks in the behavior of the entropy when we straddled the critical points of two ESQPTs. More importantly, we have shown that the difference between two types of ESQPTs can be identified by analyzing the scaling properties of the entropy. Furthermore, we have also confirmed

the ability of the entropy to detect and distinguish two ESQPTs in the energy space.

Our study extends our understanding on the properties of two ESQPTs in the anharmonic LMG model. In particular, the main results suggest that the scaling analysis of the quantum work distribution entropy is essential for detecting the differences between ESQPTs. Moreover, our findings also provide further evidence of the usefulness of the entropy in studying and diagnosing of different phase transitions in quantum many-body systems. We would like to point out that our main conclusions, despite of building on the anharmonic LMG model, are general for the ESQPTs that are characterized by the logarithmic divergence of the density of states. Whether the results in this work are still hold for other kinds of ESQPTs, such as the one defined as the nonanalytical in the first derivative of the density of states, remains an open question and deserves further exploration. Another possible extension of the present work would be to elucidate whether the finite size scaling analysis of the entropy can help us to classify various ESQPTs.

Finally, the quantum work distribution based on the two-point measurement scheme has been experimentally measured in several platforms [91–94]. We therefore hope that our findings could open up a promising way for the use of the quantum work distribution entropy in the experimental studies of ESQPTs.

ACKNOWLEDGMENTS

Q.W. acknowledges support from the Slovenian Research and Innovation Agency (ARIS) under Grants No. J1-4387 and No. P1-0306. This work was also supported by the Zhejiang Provincial Nature Science Foundation under Grants No. LQ22A040006 and No. LY20A050001 and the National Science Foundation of China under Grant No. 11805165.

-
- [1] P. Cejnar, M. Macek, S. Heinze, J. Jolie, and J. Dobeš, *J. Phys. A: Math. Gen.* **39**, L515 (2006).
 - [2] P. Cejnar and P. Stránský, *Phys. Rev. E* **78**, 031130 (2008).
 - [3] M. Caprio, P. Cejnar, and F. Iachello, *Ann. Phys.* **323**, 1106 (2008).
 - [4] P. Stránský, M. Macek, and P. Cejnar, *Ann. Phys.* **345**, 73 (2014).
 - [5] P. Cejnar, P. Stránský, M. Macek, and M. Kloc, *J. Phys. A: Math. Theor.* **54**, 133001 (2021).
 - [6] L. Carr, *Understanding Quantum Phase Transitions*, Condensed Matter Physics (CRC Press, Boca Raton, FL, 2010).
 - [7] S. Sachdev, *Quantum Phase Transitions*, 2nd ed. (Cambridge University Press, Cambridge, UK, 2011).
 - [8] T. Brandes, *Phys. Rev. E* **88**, 032133 (2013).
 - [9] M. A. Bastarrachea-Magnani, S. Lerma-Hernández, and J. G. Hirsch, *Phys. Rev. A* **89**, 032101 (2014).
 - [10] C. M. Lóbez and A. Relaño, *Phys. Rev. E* **94**, 012140 (2016).
 - [11] M. Kloc, P. Stránský, and P. Cejnar, *Phys. Rev. A* **98**, 013836 (2018).
 - [12] A. L. Corps and A. Relaño, *Phys. Rev. Lett.* **127**, 130602 (2021).
 - [13] R. Puebla, M.-J. Hwang, and M. B. Plenio, *Phys. Rev. A* **94**, 023835 (2016).
 - [14] P. Stránský, P. Cejnar, and R. Filip, *Phys. Rev. A* **104**, 053722 (2021).
 - [15] V. M. Bastidas, P. Pérez-Fernández, M. Vogl, and T. Brandes, *Phys. Rev. Lett.* **112**, 140408 (2014).
 - [16] A. Sáiz, J. Khalouf-Rivera, J. M. Arias, P. Pérez-Fernández, and J. Casado-Pascual, *arXiv:2302.00382*.
 - [17] P. Feldmann, C. Klempt, A. Smerzi, L. Santos, and M. Gessner, *Phys. Rev. Lett.* **126**, 230602 (2021).
 - [18] J. Cabedo and A. Celi, *Phys. Rev. Res.* **3**, 043215 (2021).
 - [19] Z.-X. Niu and Q. Wang, *Phys. Rev. A* **107**, 033307 (2023).
 - [20] Z.-G. Yuan, P. Zhang, S.-S. Li, J. Jing, and L.-B. Kong, *Phys. Rev. A* **85**, 044102 (2012).
 - [21] G. Engelhardt, V. M. Bastidas, W. Kopylov, and T. Brandes, *Phys. Rev. A* **91**, 013631 (2015).
 - [22] W. Kopylov and T. Brandes, *New J. Phys.* **17**, 103031 (2015).

- [23] L. F. Santos and F. Pérez-Bernal, *Phys. Rev. A* **92**, 050101(R) (2015).
- [24] M. Šindelka, L. F. Santos, and N. Moiseyev, *Phys. Rev. A* **95**, 010103(R) (2017).
- [25] Q. Wang and F. Pérez-Bernal, *Phys. Rev. A* **100**, 022118 (2019).
- [26] A. L. Corps and A. Relaño, *Phys. Rev. B* **106**, 024311 (2022).
- [27] L. F. Santos, M. Távora, and F. Pérez-Bernal, *Phys. Rev. A* **94**, 012113 (2016).
- [28] Q. Wang and F. Pérez-Bernal, *Phys. Rev. E* **103**, 032109 (2021).
- [29] J. Chávez-Carlos, T. L. M. Lezama, R. G. Cortiñas, J. Venkatraman, M. H. Devoret, V. S. Batista, F. Pérez-Bernal, and L. F. Santos, *npj Quantum Inf.* **9**, 76 (2023).
- [30] Q.-W. Wang and S. Wu, *Phys. Rev. A* **102**, 063531 (2020).
- [31] B. Dietz, F. Iachello, M. Miski-Oglu, N. Pietralla, A. Richter, L. von Smekal, and J. Wambach, *Phys. Rev. B* **88**, 104101 (2013).
- [32] B. Meyer-Hoppe, F. Anders, P. Feldmann, L. Santos, and C. Klempt, *Phys. Rev. Lett.* **131**, 243402 (2023).
- [33] A. Relaño, J. M. Arias, J. Dukelsky, J. E. García-Ramos, and P. Pérez-Fernández, *Phys. Rev. A* **78**, 060102(R) (2008).
- [34] P. Pérez-Fernández, A. Relaño, J. M. Arias, J. Dukelsky, and J. E. García-Ramos, *Phys. Rev. A* **80**, 032111 (2009).
- [35] F. Pérez-Bernal and L. F. Santos, *Fortschr. Phys.* **65**, 1600035 (2017).
- [36] Q. Wang and F. Pérez-Bernal, *Phys. Rev. A* **100**, 062113 (2019).
- [37] S. Pilatowsky-Cameo, J. Chávez-Carlos, M. A. Bastarrachea-Magnani, P. Stránský, S. Lerma-Hernández, L. F. Santos, and J. G. Hirsch, *Phys. Rev. E* **101**, 010202(R) (2020).
- [38] M. Kloc, D. Šimsa, F. Hanák, P. R. Kaprálová-Žďánská, P. Stránský, and P. Cejnar, *Phys. Rev. A* **103**, 032213 (2021).
- [39] P. Pérez-Fernández, A. Relaño, J. M. Arias, P. Cejnar, J. Dukelsky, and J. E. García-Ramos, *Phys. Rev. E* **83**, 046208 (2011).
- [40] I. García-Mata, E. Vergini, and D. A. Wisniacki, *Phys. Rev. E* **104**, L062202 (2021).
- [41] L. Zhou, J. Kong, Z. Lan, and W. Zhang, *Phys. Rev. Res.* **5**, 013087 (2023).
- [42] D. J. Nader, C. A. González-Rodríguez, and S. Lerma-Hernández, *Phys. Rev. E* **104**, 064116 (2021).
- [43] J. Khalouf-Rivera, M. Carvajal, L. F. Santos, and F. Pérez-Bernal, *J. Phys. Chem. A* **123**, 9544 (2019).
- [44] F. Pérez-Bernal and O. Álvarez-Bajo, *Phys. Rev. A* **81**, 050101(R) (2010).
- [45] J. Khalouf-Rivera, F. Pérez-Bernal, and M. Carvajal, *Phys. Rev. A* **105**, 032215 (2022).
- [46] J. Gamito, J. Khalouf-Rivera, J. M. Arias, P. Pérez-Fernández, and F. Pérez-Bernal, *Phys. Rev. E* **106**, 044125 (2022).
- [47] J. Khalouf-Rivera, J. Gamito, F. Pérez-Bernal, J. M. Arias, and P. Pérez-Fernández, *Phys. Rev. E* **107**, 064134 (2023).
- [48] A. Kiely, E. O'Connor, T. Fogarty, G. T. Landi, and S. Campbell, *Phys. Rev. Res.* **5**, L022010 (2023).
- [49] Z. Mzaouali, R. Puebla, J. Goold, M. El Baz, and S. Campbell, *Phys. Rev. E* **103**, 032145 (2021).
- [50] P. Solinas and S. Gasparinetti, *Phys. Rev. E* **92**, 042150 (2015).
- [51] R. Sampaio, S. Suomela, T. Ala-Nissila, J. Anders, and T. G. Philbin, *Phys. Rev. A* **97**, 012131 (2018).
- [52] G. Francica, *Phys. Rev. E* **105**, 014101 (2022).
- [53] G. Francica, *Phys. Rev. E* **106**, 054129 (2022).
- [54] M. Lostaglio, A. Belenchia, A. Levy, S. Hernández-Gómez, N. Fabbri, and S. Gherardini, *Quantum* **7**, 1128 (2023).
- [55] F. Cerisola, F. Mayo, and A. J. Roncaglia, *Quantum* **25**, 1439 (2023).
- [56] P. Talkner, E. Lutz, and P. Hänggi, *Phys. Rev. E* **75**, 050102(R) (2007).
- [57] H. Tasaki, [arXiv:cond-mat/0009244](https://arxiv.org/abs/cond-mat/0009244).
- [58] J. Kurchan, [arXiv:cond-mat/0007360](https://arxiv.org/abs/cond-mat/0007360).
- [59] S. Deffner and E. Lutz, *Phys. Rev. E* **77**, 021128 (2008).
- [60] A. Silva, *Phys. Rev. Lett.* **101**, 120603 (2008).
- [61] R. Dornier, J. Goold, C. Cormick, M. Paternostro, and V. Vedral, *Phys. Rev. Lett.* **109**, 160601 (2012).
- [62] J. Marino and A. Silva, *Phys. Rev. B* **89**, 024303 (2014).
- [63] S. Campbell, *Phys. Rev. B* **94**, 184403 (2016).
- [64] J. Goold, F. Plastina, A. Gambassi, and A. Silva, The role of quantum work statistics in many-body physics, in *Thermodynamics in the Quantum Regime: Fundamental Aspects and New Directions*, edited by F. Binder, L. A. Correa, C. Gogolin, J. Anders, and G. Adesso (Springer International Publishing, Cham, 2018), pp. 317–336.
- [65] Z. Fei, N. Freitas, V. Cavina, H. T. Quan, and M. Esposito, *Phys. Rev. Lett.* **124**, 170603 (2020).
- [66] K. Zawadzki, A. Kiely, G. T. Landi, and S. Campbell, *Phys. Rev. A* **107**, 012209 (2023).
- [67] K. Zawadzki, R. M. Serra, and I. D'Amico, *Phys. Rev. Res.* **2**, 033167 (2020).
- [68] L. Fusco, S. Pigeon, T. J. G. Apollaro, A. Xuereb, L. Mazzola, M. Campisi, A. Ferraro, M. Paternostro, and G. De Chiara, *Phys. Rev. X* **4**, 031029 (2014).
- [69] Q. Wang and H. T. Quan, *Phys. Rev. E* **96**, 032142 (2017).
- [70] H. Lipkin, N. Meshkov, and A. Glick, *Nucl. Phys.* **62**, 188 (1965).
- [71] N. Meshkov, A. Glick, and H. Lipkin, *Nucl. Phys.* **62**, 199 (1965).
- [72] A. Glick, H. Lipkin, and N. Meshkov, *Nucl. Phys.* **62**, 211 (1965).
- [73] S. Dusuel and J. Vidal, *Phys. Rev. Lett.* **93**, 237204 (2004).
- [74] S. Dusuel and J. Vidal, *Phys. Rev. B* **71**, 224420 (2005).
- [75] O. Castaños, R. López-Peña, J. G. Hirsch, and E. López-Moreno, *Phys. Rev. B* **74**, 104118 (2006).
- [76] P. Ribeiro, J. Vidal, and R. Mosseri, *Phys. Rev. Lett.* **99**, 050402 (2007).
- [77] P. Ribeiro, J. Vidal, and R. Mosseri, *Phys. Rev. E* **78**, 021106 (2008).
- [78] S. Campbell, G. De Chiara, M. Paternostro, G. M. Palma, and R. Fazio, *Phys. Rev. Lett.* **114**, 177206 (2015).
- [79] A. Russomanno, F. Iemini, M. Dalmonte, and R. Fazio, *Phys. Rev. B* **95**, 214307 (2017).
- [80] Z.-Z. Zhang and W. Wu, *Phys. Rev. E* **106**, 034104 (2022).
- [81] M. Afrasiar, J. K. Basak, B. Dey, K. Pal, and K. Pal, *J. Stat. Mech.* (2023) 103101.
- [82] M. Kumari and Á. M. Alhambra, *Quantum* **6**, 701 (2022).
- [83] T. Zibold, E. Nicklas, C. Gross, and M. K. Oberthaler, *Phys. Rev. Lett.* **105**, 204101 (2010).
- [84] J. A. Muniz, D. Barberena, R. J. Lewis-Swan, D. J. Young, J. R. K. Cline, A. M. Rey, and J. K. Thompson, *Nature (London)* **580**, 602 (2020).
- [85] K. Xu, Z.-H. Sun, W. Liu, Y.-R. Zhang, H. Li, H. Dong, W. Ren, P. Zhang, F. Nori, D. Zheng, H. Fan, and H. Wang, *Sci. Adv.* **6** (2020).

- [86] J. M. Radcliffe, *J. Phys. A: Gen. Phys.* **4**, 313 (1971).
- [87] W.-M. Zhang, D. H. Feng, and R. Gilmore, *Rev. Mod. Phys.* **62**, 867 (1990).
- [88] J.-P. Gazeau, *Coherent States in Quantum Optics* (Wiley-VCH, Berlin, 2009).
- [89] A. Perelomov, *Generalized Coherent States and Their Applications* (Springer, Berlin, 2012).
- [90] M. Gutzwiller, *Chaos in Classical and Quantum Mechanics*, Interdisciplinary Applied Mathematics (Springer, New York, NY, 2013).
- [91] R. Dornier, S. R. Clark, L. Heaney, R. Fazio, J. Goold, and V. Vedral, *Phys. Rev. Lett.* **110**, 230601 (2013).
- [92] L. Mazzola, G. De Chiara, and M. Paternostro, *Phys. Rev. Lett.* **110**, 230602 (2013).
- [93] T. B. Batalhão, A. M. Souza, L. Mazzola, R. Auccaise, R. S. Sarthour, I. S. Oliveira, J. Goold, G. De Chiara, M. Paternostro, and R. M. Serra, *Phys. Rev. Lett.* **113**, 140601 (2014).
- [94] S. An, J.-N. Zhang, M. Um, D. Lv, Y. Lu, J. Zhang, Z.-Q. Yin, H. T. Quan, and K. Kim, *Nat. Phys.* **11**, 193 (2015).